Macromolecules

ARTICLE

pubs.acs.org/Macromolecules

Self-Nucleation of Polymers with Flow: The Case of Bimodal Polyethylene

Luigi Balzano,[†,⊥] Sanjay Rastogi,[§,⊥] and Gerrit Peters[*,‡,⊥]

[†]Department of Chemical Engineering, Eindhoven University of Technology, P.O. Box 513, 5600MB, Eindhoven, The Netherlands

[‡]Department of Mechanical Engineering, Eindhoven University of Technology, P.O. Box 513, 5600MB, Eindhoven, The Netherlands

[§]Department of Materials, Loughborough University, Loughborough LE11 3TU, United Kingdom

[⊥]Dutch Polymer Institute (DPI), PO Box 902, 5600 AX Eindhoven, The Netherlands

ABSTRACT: A small amount of high molecular weight molecules can have a dramatic influence on the flow-induced crystallization kinetics and morphology of polymers. In this paper, it is shown that with the addition of 7 wt % of high molecular weight molecules a melt of low molecular weight polyethylene can be tailored for process-induced self-nucleation. To ensure mixing between molecules of high and low molecular weight, we make use of a special synthesis route where both fractions are generated simultaneously by two catalysts immobilized on the same support. Under the influence of flow, the high molecular weight molecules make crystallization possible at temperatures as high as 137 °C, where the matrix alone cannot crystallize. Moreover, flow can lead to fibrillar precursors of crystallization at temperatures as high as 142 °C, i.e., in the vicinity of the equilibrium melting point. On cooling below 139 °C, these precursors crystallize and transform into shishes while the growth of kebabs is still suppressed because of the high temperature. With exact lattice matching and an excellent state of dispersion, shishes generated at this high temperature are ideal as a substrate for heterogeneous crystallization (self-nucleation). In fact, with the processing conditions explored here, they can shift the onset of crystallization, 124 °C in quiescent conditions, up to temperatures as high as 132 °C during cooling at 5 °C/min. The effect of shear at 142 °C on the nonisothermal crystallization of the material is explored varying systematically shear rate and shear time. These novel findings on self-nucleation also demonstrate that the crystallization temperature of polymers is a processing parameter that depends on the whole thermomechanical history and not only on the cooling rate. In particular, for the bimodal polyethylene investigated in this work, after shear at 142 °C, the crystallization temperature and other crystallization parameters are governed essentially by the macroscopic strain.

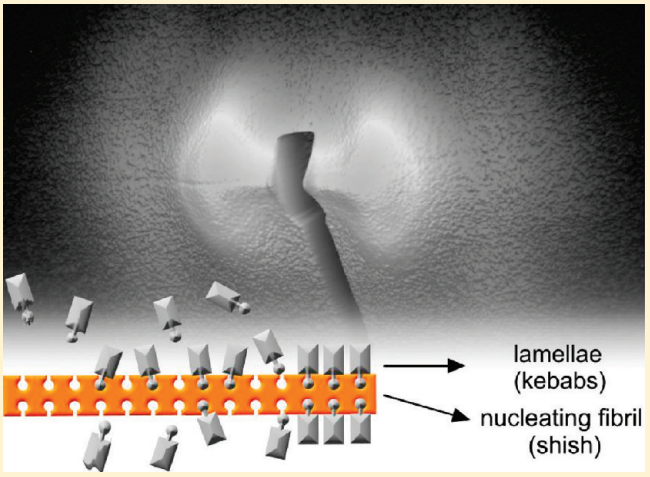

INTRODUCTION

Nucleation is the limiting step of crystallization kinetics in polymers. According to classical theories, homogeneous nucleation takes place because of density fluctuations.[1] From a molecular point of view, density fluctuations are transient clusters of molecular segments that form at all temperatures because of Brownian motion. The formation of a cluster leads to a change in the Gibbs free energy of the system: $\Delta G = \Delta G_V + \Delta G_S$,[2] where ΔG_V is the energy gained because of the increased order and ΔG_S is the work needed to build the new interface between the cluster and the melt. In undercooled melts, the stability of a cluster is governed by the balance between ΔG_V and ΔG_S that leads to a critical size. For small clusters (below the critical size), the interfacial term ΔG_S dominates, and this prevents stabilization and further growth. Therefore, small clusters are unstable and dissolve back to the melt. Occasionally, clusters can grow above the critical size and become stable as the low surface to volume ratio makes ΔG_V the dominating factor. From this moment onward, further growth decreases Gibbs free energy and is a spontaneous process. In practice, during bulk crystallization, homogeneous nucleation never takes place. Nucleation at the interface with foreign particles (contaminants or purposely added) is much more favored and always dominates structure formation. Particle-assisted nucleation is commonly referred to as heterogeneous and is further discussed in this paper.

Besides being an interesting scientific topic, nucleation in polymers is an important industrial issue as well. Slow nucleation can limit cycle times and is economically not attractive. To

Received: November 23, 2010
Revised: February 15, 2011
Published: March 23, 2011

dx.doi.org/10.1021/ma102662p | *Macromolecules* 2011, 44, 2926–2933

overcome this issue, nucleation is often speeded up with nucleating agents, low molecular weight compounds, or polymers that are blended-in during processing. The role of these compounds is to reduce ΔG_S, the energy needed to build new interfaces during nucleation and, thus, decrease the critical size for the activation of spontaneous growth. As a consequence, when cooling from the melt, crystallization can take place at a higher temperature and the number of nuclei increases.[3−5] To reduce ΔG_S, nucleating agents rest on local van der Waals interactions with polymer molecules. A good interaction takes place when the nucleating agent is crystalline because, in this case, the contact surface has a regular pattern. When the lattice parameters of the interface are close to those of the overgrowing crystals, polymer molecules are even more stimulated to adopt configurations that favor nucleation.[6] Efficient nucleating agents have been found for a number of polymers.[7−12] The strongest effects are observed when the mismatch between lattice parameters at the contact interface is less than 15%.[13] Considered this tight tolerance, crystalline seeds of the polymer itself, with no lattice mismatch, have unsurpassable efficiency. Heterogeneous nucleation starting from crystalline seeds of the polymer itself is called self-nucleation and is feasible under the condition that a method to generate crystalline seeds at high temperatures is available. Banks et al.,[14] Blundell et al.,[15] and Fillon et al.[16] generated crystallization seeds close to the nominal melting point by applying tailored thermal histories to the solid material. In particular, Fillon et al.[16] report that seeds obtained from the fragmentation of partially molten crystals can increase the crystallization temperature of isotactic polypropylene up to 25 °C and, at the same time, increase the number of nuclei by several orders. Such observations disclose the potential of self-nucleation. However, so far, literature describes essentially the case of seeds obtained via tailored thermal treatments of the solid material, ignoring that crystallization seeds can be obtained also from a melt by making use of flow-induced crystallization.[17−22] This latter strategy, based on stretching molecules, permits the formation of crystallization seeds at temperatures higher than the nominal melting point[23−26] and, sometimes, even higher than the equilibrium melting point.[27−29] In particular, we have recently shown that, for polyethylene (PE), shear in the vicinity of the equilibrium melting point can lead to a suspension of dense fibrils with little crystallinity and diameter around 30 nm[30] that, due to the extended-chain structure, can further crystallize becoming potential seeds for self-nucleation. The effect of flow conditions on the formation of seeds at high temperature and their nucleating performance are largely unexplored and are the topic of this paper. In the first part, we show that seeds of crystallization can be generated at high temperature from a relatively low molecular weight PE matrix by the addition of a high molecular weight tail. In the second part, we analyze the nucleating ability of fibrillar seeds that form on cooling after shear in the vicinity of the equilibrium melting point.

MATERIALS AND METHODS

Time-Resolved X-ray Measurements. Small-angle X-ray scattering (SAXS) was carried out at the beamline ID02 of European Synchrotron Radiation Facility (Grenoble, France) with wavelength $\lambda = 1.24$ Å. Two-dimensional images, recorded every 3 s at a distance of about 2.7 m from the sample, were corrected for beam intensity and scattering of the empty sample cell. The scattered intensity was then plotted against the magnitude of the scattering vector $q = (4\pi/\lambda)\sin\theta$, where 2θ is the scattering angle. The integrated intensity as a function of ξ (temperature or time) was defined as $I(\xi) = \int_{q_{min}}^{q_{max}} I(q;\xi)\,dq$, with q_{min} and q_{max} the minimum and maximum accessible q values, respectively.[31] After crystallization, the degree of lamellar orientation was estimated from the value of the Hermans' orientation factor $F_H^{SAXS} = (3\langle\cos^2\varphi\rangle - 1)/2$, where $\langle\cos^2\varphi\rangle$, the average cosine squared of the angle between the perpendicular to the lamellar stacks and the flow direction, is given by $\langle\cos^2\varphi\rangle = (\int_0^{\pi/2} I(\beta)\cos^2\beta\sin\beta\,d\beta)/(\int_0^{\pi/2} I(\beta)\sin\beta\,d\beta)$, where β represents the azimuthal angle (in radians) on the two-dimensional images.

Wide-angle X-ray diffraction (WAXD) was performed at the beamline BM26 of the European Synchrotron Radiation Facility (Grenoble, France). Two-dimensional images were recorded with a Frelon detector and corrected for spatial distortion and for the scattering of the empty sample cell. Afterward, the profiles of intensity versus scattering angle (2θ) were normalized with respect to the total scattered intensity $I_{WAXD}^{tot}(\xi) = \int_{2\theta_{min}}^{2\theta_{max}} I_{WAXD}(2\theta;\xi)\,d(2\theta)$. The crystallinity index was calculated after deconvolution of the intensity scattered by the amorphous (I_A) and by the crystalline phase (I_C) using procedures suggested in the literature:[32] $x = 100 \times I_C/(I_C + I_A)$.

Flow Cell. Shear flow experiments were performed in combination with X-ray using a Linkam shear cell CSS-450. To reduce unwanted scattering, the original material of the windows was replaced with Kapton. Before performing the experiments, samples (compression molded disks with thickness of about 200 μm) were annealed for 3 min at 200 °C in order to erase the memory of previous thermomechanical histories.

Rheological Time Scales. From a rheological point of view, the effect of flow on molecular conformation can be assessed defining Weissenberg numbers for molecular orientation and stretch: $Wi_o = \tau_D\dot{\gamma}$ and $Wi_s = \tau_S\dot{\gamma}$, with $\dot{\gamma}$ being the shear rate and τ_D and τ_S the disengagement and the stretch relaxation time, respectively. During shear, molecules tend to orient for values of $Wi_o > 1$ and to stretch for values of $Wi_s > 1$. When dynamic dilution can be excluded (like for the materials used in this work, as demonstrated in ref 30), the relaxation time of molecules with mass M can be calculated using relations from the tube model of Doi and Edwards:[33]

$$\tau_s = \tau_e(M/M_e)^2 \tag{1.1}$$

$$\tau_D = 3\tau_e(M/M_e)^3(1 - 1.51/\sqrt{M/M_e})^2 \tag{1.2}$$

with $M_e = 828$ g/mol the average molecular weight between entanglements and τ_e the entanglement equilibration time that for PE is 7×10^{-9} s at 190 °C.[34] In the following, the symbols τ_D^w and τ_S^w are used when $M = M_w$ and the symbols τ_D^Z and τ_S^Z when $M = M_Z$. Given a molar mass M, the relations 1.1 and 1.2 together with an Arrhenius type of temperature dependence (with $E_a = 36$ kJ/mol) allow for calculation of the relaxation times at all temperatures.

Crystallization Kinetics. Crystallization kinetics can be investigated by means of the Avrami model[35−37] that describes the space filling as a function of time, $\Phi(t)$. The model is expressed by the relation

$$\Phi(t) = 1 - \exp[-kt^n] \tag{1.3}$$

where k is a rate parameter and n indicates the geometry of the growing crystallites. In isothermal conditions, k is a constant and the Avrami equation (1.3), rewritten as $\ln[-\ln(1-\Phi)] = \ln(k) + n\ln(t)$, predicts that $\ln[-\ln(1-\Phi)]$ versus $\ln(t)$ (Avrami plot) is a straight line with slope n. The model postulates integer values of n when a single space-filling process is active. Values of n relevant to this paper are $n = 3$ obtained when the space is filled by spherulites (three-dimensional growth front) and $n = 2$ obtained when the space is filled by kebabs (two-dimensional growth front). Both cases refer to preformed nuclei; i.e., all nuclei are already present at the reference time ($t = 0$), and no nucleation

takes place afterward (during growth). Fractional values of n are possible when more than one space-filling process is active.[38]

The space filling Φ can be calculated assuming proportionality with WAXD crystallinity: $\Phi = (x - x_0)/(x_\infty - x_0)$ where x_0 is the crystallinity at $t = 0$, i.e., immediately after flow, and x_∞ is the plateau crystallinity attained at very long times. With this definition, the model can only describe changes in crystallinity that correspond to changes in the space filling, i.e., primary crystallization. Secondary crystallization, which takes place (at long times) behind the growth front, i.e., not changing space filling, is not captured.

RESULTS AND DISCUSSION

Two linear high-density polyethylenes (PE) with different molecular weight distribution are specially synthesized for this research. PE1 is synthesized using a chromium-based catalyst and PE2 with a combination of the same chromium-based catalyst and an iron-based catalyst. The chromium-based catalyst leads to relatively low molecular weight PE, while the iron-based catalyst to high molecular weight PE. Details about synthesis and rheological properties of the materials are given by Kukalyekar et al.[39,40] In both cases, the chosen synthesis conditions together with the sample preparation protocol lead to well-entangled polymers. As shown in Table 1, the overall M_w of PE1 and PE2 differ by a factor less than 2. Nevertheless, because of the higher polydispersity, M_Z of PE2 is about 10 times higher than M_Z of PE1.

A closer look at the GPC traces, shown in Figure 1, shows that PE1 exhibit a unimodal molecular weight distribution, whereas PE2 exhibits a bimodal molecular weight distribution with a low and a high molecular weight fraction (LMW and HMW).

When PE2 is described with the weighted sum of two log-normal distributions, the best-fit parameters, given in Table 2, indicate that M_w of the LMW component is 5.5×10^4 g/mol, close to the M_w of PE1, and M_w of the HMW component is 1.1×10^6 g/mol. Therefore, the bimodal PE2 can be considered as obtained from PE1 with the addition of the HMW fraction. The synthesis of this material with two catalysts producing LMW and HMW simultaneously ensures that, despite the large difference in molar mass, the two fractions are molecularly mixed.

Table 1. Overall Molecular Weight Parameters for PE1 and PE2

	M_w [g/mol]	M_w/M_n	M_Z [g/mol]
PE1	7×10^4	3.5	2.4×10^5
PE2	12.8×10^4	7.4	1.6×10^6

The critical overlap concentration of HMW molecules is about 0.5 wt %. Therefore, in PE2, with a concentration of 7 wt %, HMW molecules are well entangled among them. The relaxation times of HMW molecules at 142 °C are $\tau_D^w \simeq 140$ s and $\tau_S^w \simeq 0.04$ s, based on M_w, and $\tau_D^Z \simeq 1630$ s and $\tau_S^Z \simeq 0.19$ s, based on M_Z.

Isothermal Flow-Induced Crystallization. Temperature has a large influence on crystallization.[41,42] Nucleation and growth rates vanish at low undercoolings and make crystallization close to the melting point unlikely in quiescent conditions. For PE, literature data do not go beyond 132 °C.[43] Nevertheless, in the following, we show that remarkable effects can be observed even above this temperature, when sufficient strong flow is applied. For simplicity, we use the same shear conditions, 30 s^{-1} for 2 s, for PE1 and PE2, and crystallization is studied isothermally at different temperatures. As observed in Figure 2a, at 129 °C, PE1 reaches a plateau crystallinity of about 40% after ~500 s. The plateau crystallinity drops to ~5% at 132 °C, and eventually, at 137 °C, the material no longer crystallizes within the 1000 s of experimental time (data not shown). The uniform azimuthal distribution of WAXD intensity at 129 and at 132 °C indicates that crystals develop with no preferential orientation and, therefore, assemble in spherulites. At 129 °C, this is confirmed by the Avrami exponent $n = 2.96 \pm 0.25$ (see Figure 3). At 132 °C, the low crystallinity indicates incomplete space filling and makes unreliable the value of n; therefore, growth of spherulites cannot be confirmed with WAXD data.

PE2 exhibits much faster crystallization kinetics than PE1. As shown in Figure 2b, the plateau crystallinity is attained at shorter times. Remarkably, with the presence of HMW molecules, PE2 can crystallize at temperatures as high as 137 °C. The nonuniform WAXD intensity, with equatorial arching of the 110 and 200 reflections (see inset of Figure 2b), indicates that crystals are preferentially oriented in the flow direction. At 133 °C, this circumstance, in combination with the Avrami exponent n close to 2 (see Figure 3), indicates the growth of lamellar stacks oriented in the flow direction (kebabs).

At this point, it is important to note that, within the experimental time (1000 s), both PE1 and PE2 do not crystallize without the application of flow in the temperature range 129−137 °C. Consequently, the crystallites of Figure 2 can be regarded as the result of a self-nucleation process initiated by flow-induced seeds of crystallization. The difference between PE1 and PE2 lies in the concentration and morphology of the flow-induced seeds. Concerning morphology, shear on the low molecular weight (unimodal) PE1 leads to pointlike seeds that

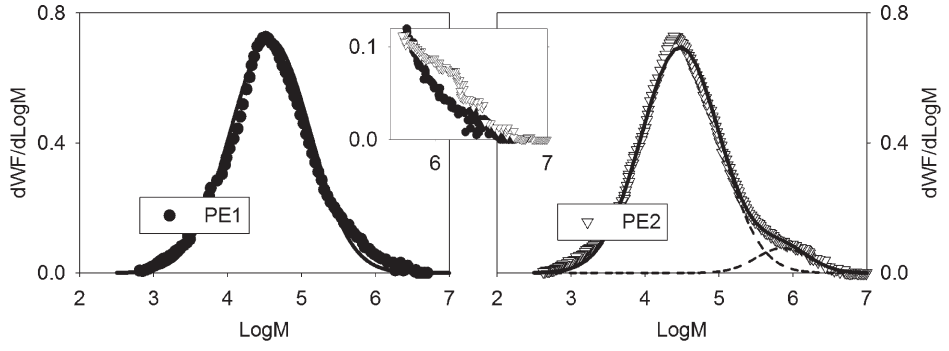

Figure 1. GPC traces of PE1 (left) and PE2 (right). The lines represent fitted log-normal distributions. The inset shows a detail of the graph obtained overlapping the two distributions in the high molecular weight region.

Table 2. Detailed Molecular Weight Parameters for PE2

	LMW M_w [g/mol]	LMW M_w/M_n	LMW M_Z [g/mol]	HMW M_w [g/mol]	HMW M_w/M_n	HMW M_Z [g/mol]	HMW [wt %]
PE2	5.5×10^4	3.5	1.9×10^5	1.1×10^6	2.3	2.5×10^6	7

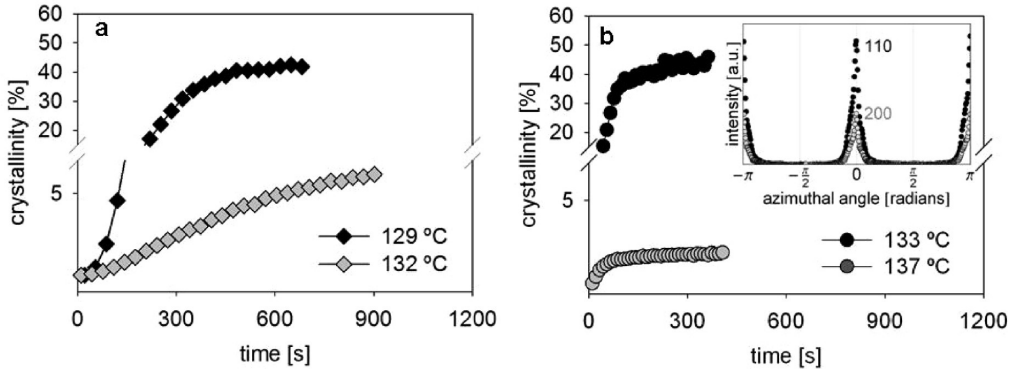

Figure 2. Crystallinity during isothermal crystallization after a pulse of shear of 30 s^{-1} for 2 s: (a) for PE1 and (b) for PE2.

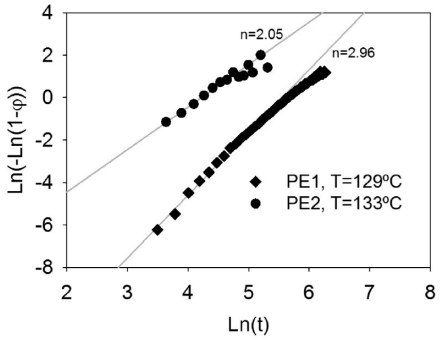

Figure 3. Avrami plots for PE1 at 129 °C (best fit parameters $n = 2.96$ and $\ln(k) = -16.4$) and for PE2 at 133 °C ($n = 2.05$ and $\ln(k) = -8.44$).

can initiate the growth of spherulites up to 133 °C. Whereas, shear on the bimodal PE2 leads to fibrillar, shish type, of seeds that can initiate the growth of kebabs at temperatures as high as 133 °C.

Origin of Fibrillar Flow-Induced Seeds of Crystallization. Fibrillar seeds of crystallization are easily formed in the bimodal PE2 as the HMW molecules, with their long relaxation times, are easily oriented and stretched during flow and, via the entanglements, promote similar change of conformation in neighboring molecules.[44] This cooperative change of conformation accelerates nucleation to the point that molecules can be frozen in fibrillar precursors of crystallization before they can relax back to a coiled configuration.[45] Not all fibrillar precursors can crystallize. Size plays a crucial role in discerning between precursors that crystallize or dissolve. Recently, we demonstrated that in the bimodal PE2, fibrillar precursors can be formed with shear even at 142 °C, close to the equilibrium melting point. Despite the high temperature, the largest precursors can crystallize whereas the smallest tend to dissolve.[30] As often observed, dissolution is a relatively slow process,[20,46,47] and we noticed that, initially, the characteristic dissolution time matches τ_D^w of the HMW. This implies that small precursors, i.e., precursors whose development stopped in the early stages (perhaps because they formed just before flow ceased), have a scaffold mainly of HMW molecules. In fact, being the concentration of HMW molecules in PE2 far above the critical overlap concentration, under flow, with high orientation and stretch, the probability that HMW molecules find each other in conformations suitable for nucleating precursors is significant. In a later stage, these early precursors rapidly grow in length and incorporate both HMW and LMW molecules. Eventually, as shown by Kimata et al.,[48] shishes contain an amount of HMW similar to the unperturbed melt.

Nonisothermal Crystallization of PE2 after Shear Pulse at 142 °C. At 142 °C, the dissolution time of fibrillar precursors is about 140 s. Consequently, by decreasing the temperature at a rate of 5 °C/min after the application of shear, most of the precursors can be stabilized by crystallization and transformed into shishes. It is well-known that the formation of shishes is influenced by the deformation history.[19,25,29,45,49−53] In this paragraph, we investigate the effect of shear conditions on the nucleating effect of shish-like seeds. The shear conditions are designed to sort the experiments by the macroscopic sample strain $\gamma = \dot{\gamma} t_s$, where $\dot{\gamma}$ is the shear rate and t_s the shear time. Under the hypothesis that no change of the relaxation behavior occurs due to structure formation during shear, the Weissenberg numbers of HMW molecules, based on M_w ($= 1.1 \times 10^6$ g/mol) and M_Z ($= 2.5 \times 10^6$ g/mol), corresponding to the performed experiments are given in Table 3.

SAXS images recorded just after shear, shown in Figure 4, indicate that γ governs the formation of fibrillar precursor at 142 °C.

When $\gamma = 100$, independent of the deformation history, a streak of intensity appears at the equator, and therefore, a peak is observed in the azimuthal profiles about the reference azimuthal angle. The equatorial streak indicates that, for all experiments with $\gamma = 100$, a large number of fibrillar precursors with random lateral spacing is formed.[54−57]

The shear rate independent formation of precursors suggests that the high molecular weight molecules, with their long relaxation times, cannot relax on the time scale of the experiments. Hence, they are aligned and stretched even at low shear rates, and the only requirement to form fibrillar precursors is attaining sufficient molecular deformation or, equivalently, shearing for sufficiently long time. Interestingly, Wi_s^z (Wi_s of HMW

based on M_Z) seems to capture the experimental observations better than Wi_s^w (Wi_s of HMW based on M_w). For instance, Wi_s^w suggests only a small average chain stretch for the experiments with shear rate of 5 or 25 s^{-1}, and this is not in agreement with the equatorial streak that is clearly observed when the shear time is 20 or 4 s, respectively. This discrepancy can be a consequence of polydispersity in the HMW and suggests that M_w is not representative of the entire fraction, whereas M_Z, which accounts for the longest molecules, is. However, a change in the relaxation time due to structures formed during shear cannot be ruled out a priori, especially in the experiments with the lowest shear rates and the longest shear times.

When $\gamma < 100$, the equatorial streak is never observed. Generally speaking, this is not sufficient to exclude the formation of fibrillar precursors of crystallization that can still be formed, although in lower concentration and smaller size. Nevertheless, the data of Figure 4 demonstrate that, for PE2, massive formation of fibrillar precursors requires a molecular deformation exceeding a critical threshold. At 142 °C, this threshold is attained when the macroscopic deformation is between $\gamma = 50$ and $\gamma = 100$. Below the critical threshold, the stretch ratio of the HMW molecules is insufficient to form fibrillar precursors that can give an observable equatorial streak, regardless of the shear rate.

During cooling, precursors generated with $\gamma = 100$ are stabilized by crystallization already at 139 °C as indicated by the increase of the equatorial intensity in Figure 5a, while the growth of kebabs is still suppressed because of the high temperature

The subsequent increase in equatorial intensity, during cooling, is the result of self-nucleation of kebabs. Because of the flow orientation of these lamellar stacks, nucleation of kebabs process is better observed from the meridional intensity in Figure 5b. When $\gamma = 100$, self-nucleation of kebabs starts at temperatures as high as 132 °C. For comparison, in quiescent conditions, the nucleation of lamellae stacks takes place at 124 °C.

Similar to nucleating agents, the onset temperatures of kebabs (lamellar stacks), T_c, can be used to judge the nucleating ability of fibrillar crystallization seeds. Higher T_c corresponds to better nucleation ability. As shown in Figure 6a, after shear at 142 °C, T_c of PE2 varies from 125 to 132 °C and is controlled by the macroscopic strain. In general, T_c depends on the quality (interface between nucleating substrate and polymer) and on the specific surface of the nucleating substrate. Here, it is a reasonable assumption that the quality of the seeds for self-nucleation does not depend on the deformation history; hence, T_c is governed only by their specific surface. The highest T_c values are observed for $\gamma = 100$, suggesting that, in these conditions, precursors have the largest total surface.

Figure 6b shows that the effect of flow at 142 °C on T_c tends to saturate, and when $\gamma = 100$, the maximum is nearly reached. Application of a larger macroscopic strain is likely to yield only a small increase in T_c.

The SAXS images of Figure 7, recorded at room temperature, show that during self-nucleation the orientation of the crystallization seeds is transferred to the lamellar stacks. This feature is common to some synthetic nucleating agents with fibrillar particles[58−60] and indicates that self-nucleation is much more favored than homogeneous nucleation.

Also, the degree of lamellar orientation, shown in Figure 8a, is governed by the macroscopic strain at 142 °C. Samples sheared with $\gamma = 100$ exhibit the highest degree of lamellar orientation followed by those with $\gamma = 50$ and, eventually, those with $\gamma = 25$. The substantial degree of orientation measured after cooling

Table 3. Weissenberg Numbers Based on M_w and M_Z for the HMW Fraction Sheared at 142 °C

	with $M = M_w$		with $M = M_Z$	
	Wi_s^w	Wi_o^w	Wi_s^z	Wi_s^z
100 s^{-1}	3.5	1.3×10^4	18.9	1.6×10^5
50 s^{-1}	1.8	6.5×10^3	9.5	8.1×10^4
25 s^{-1}	0.9	3.2×10^3	4.7	4.0×10^4
10 s^{-1}	0.4	1.3×10^3	1.9	1.6×10^4
5 s^{-1}	0.2	6.5×10^2	0.9	8.1×10^3
2 s^{-1}	0.07	2.6×10^2	0.4	3.2×10^3

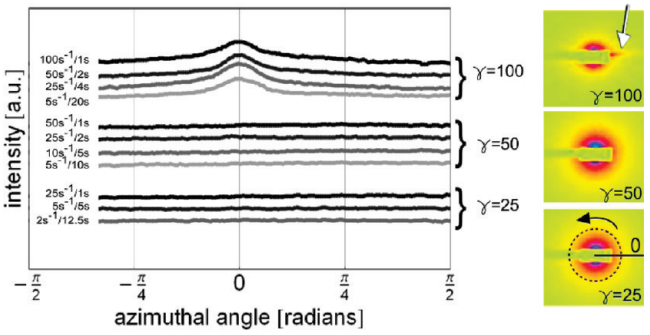

Figure 4. Azimuthal profiles of SAXS images (at $q = 0.18$ nm^{-1}) recorded immediately after application of shear at 142 °C. Experiments are sorted by the shear strain, and representative images are shown on the right-hand side. The flow direction is vertical in real space.

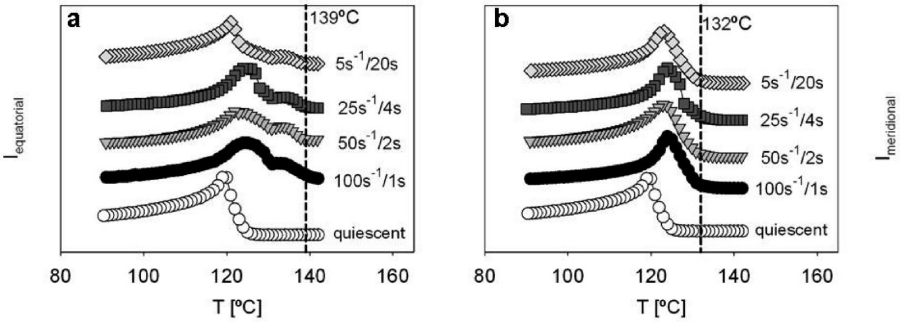

Figure 5. (a) SAXS equatorial intensity and (b) SAXS meridional intensity as a function of the temperature during cooling at 5 °C/min. Curves are shifted vertically for clarity.

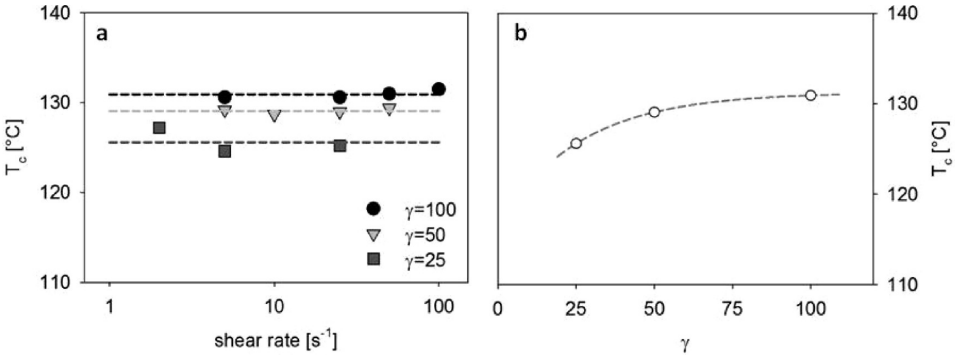

Figure 6. (a) Crystallization onset temperature during cooling at 5 °C/min measured from meridional intensity at different shear. For comparison, in quiescent conditions T_c = 124 °C. (b) Average crystallization onset temperature as a function of macroscopic sample strain at 142 °C. The dashed line is a visual guide.

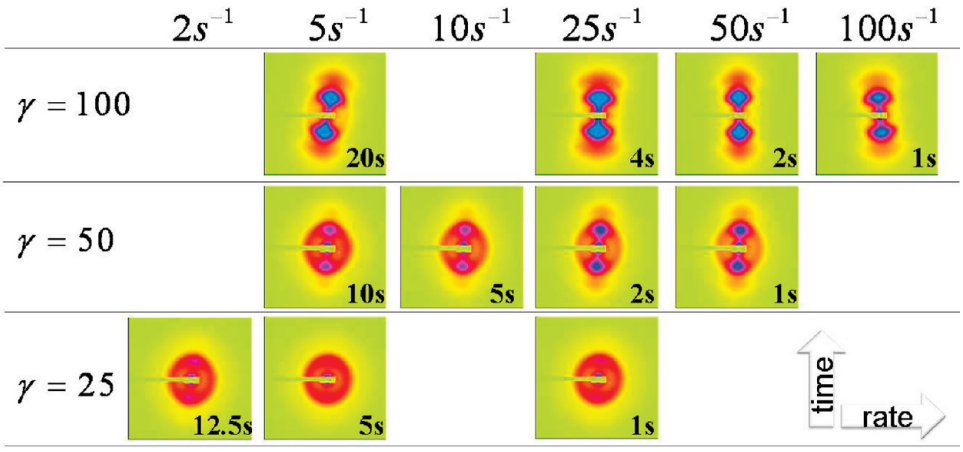

Figure 7. SAXS images recorded at room temperature after the application of shear at 142 °C and cooling at 5 °C/min. The flow direction is vertical in real space. The numbers on the images indicate the shear times.

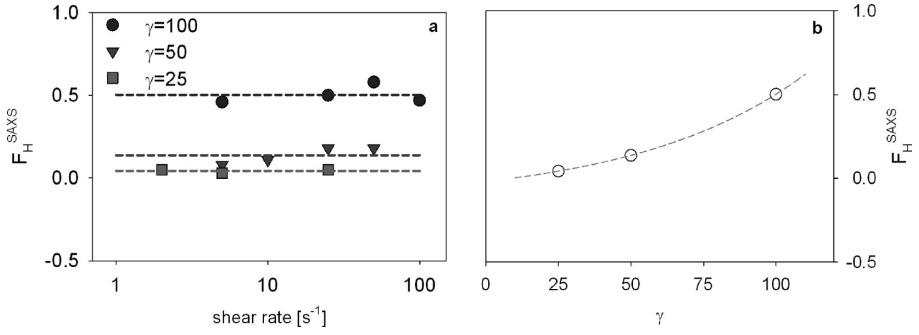

Figure 8. (a) Degree of lamellar orientation measured by SAXS at room temperature after shear at 142 °C and cooling at 5 °C/min. (b) Average degree of lamellar orientation at room temperature as a function of macroscopic sample strain at 142 °C. The dashed line is a visual guide.

when γ = 50 suggests that, similar to γ = 100 and notwithstanding the absence of an equatorial streak, shear promotes fibrillar precursors that on cooling become crystallization seeds able to transfer their orientation to the developing lamellar stacks.

Despite the effect of shear at 142 °C on T_c tends to saturate at increasing strain; the opposite is true for the degree of lamellar orientation. In fact, Figure 8b shows that with increasing strain steadily higher degrees of lamellar orientation are obtained.

Self-nucleation increases T_c and, therefore, has influence on lamellar thickness as well.[2,61] During cooling, lamellae nucleated at high temperature are annealed too, and therefore have the opportunity of growing thicker. Figure 9a shows that with increasing macroscopic strain at 142 °C, as a result of thicker lamellae, the first- and second-order SAXS peaks, at room temperature, shift toward lower q values, and the corresponding long periods, reported in Figure 9b as a function of the

dx.doi.org/10.1021/ma102662p |*Macromolecules* 2011, 44, 2926–2933

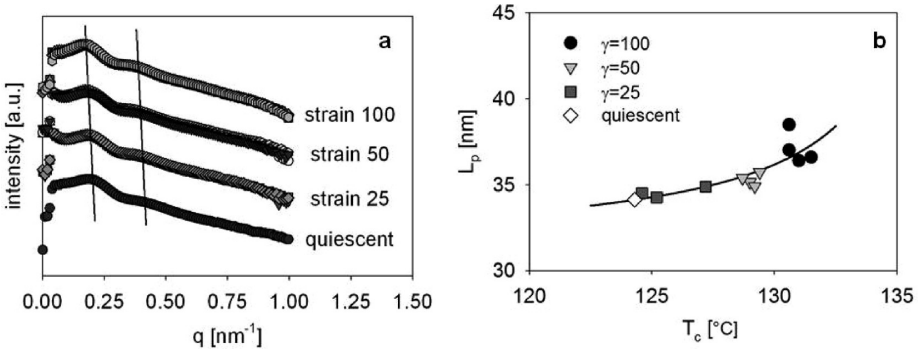

Figure 9. (a) Meridional SAXS profiles at room temperature after shear at 142 °C and cooling at 5 °C/min. The thick lines indicate the positions of the first and second order peaks. (b) Long periods at room temperature as a function of the crystallization temperature after pulse of shear at 142 °C. The line represents the fit with eq 1.4.

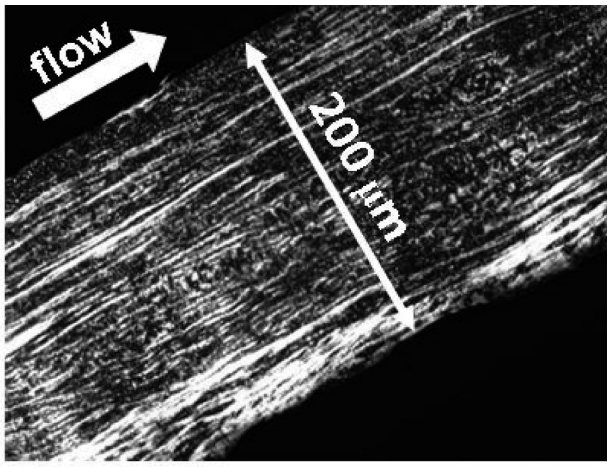

Figure 10. Cross-polarized optical micrograph of microtomed slices of the sample sheared at 142 °C with 100 s^{-1} for 1 s.

crystallization temperature, suggest that the effect of the crystallization temperature becomes more pronounced above 130 °C.

The long period as a function of the crystallization temperature can be described with the empirical relation[62]

$$L_p = C_1 + \frac{C_2}{T_m - T_c} \qquad (1.4)$$

with C_1 = 31.2 nm, C_2 = −39.4 °C nm, and T_m = 138 °C. This suggests that, for PE2, the minimum expected long period (at very large undercoolings) is 31.2 nm and the melting point of the kebabs is 138 °C.

To finish, it is remarkable to observe that the morphological effects of shear at 142 °C are also evident at large length scales. As shown in Figure 10, for the experiment with a shear of 100 s^{-1} for 1 s, after cooling to room temperature, very long and birefringent fibrillar structures (shish-kebabs) are visible with optical microscopy in the vorticity (1−2) direction.

Combining the information on Figure 6b, Figure 8b, and Figure 9b, it can be concluded that when the concentration of high molecular weight molecules is high enough, like in PE2, kinetics (T_c) and structural features (F_H and crystal thickness) of the self-nucleated material are controlled by the macroscopic sample strain γ. For PE2, the deformation history at 142 °C can be classified in three regimes: (i) small macroscopic strain (γ = 25): small effect on T_c and F_H; (ii) intermediate macroscopic strain (γ = 50): large effect on T_c, small effect on F_H; (iii) large macroscopic strain (γ = 100): large effect on T_c and F_H and thicker crystals.

CONCLUSIONS

The high molecular weight tail of the molecular weight distribution can dramatically change kinetics and morphology when crystallization of polymers takes place under the influence of flow. In bimodal polyethylene, 7 wt % of high molecular weight molecules in a low molecular weight matrix shifts upward the temperature where the formation of anisotropic structures is possible. In particular, at 142 °C, just about the equilibrium melting point, a suspension of fibrillar precursors of crystallization can be obtained with a pulse of shear. Systematic variation of shear conditions at 142 °C suggests that, for a melt with a concentration of very long molecules far above the critical overlap concentration, the formation of the fibrillar precursors is essentially governed by the macroscopic strain. In fact, when the long molecules cannot relax on the time scales of the experiments, the only requirement for the formation of fibrillar precursors is overcoming a critical molecular deformation. On cooling below 139 °C, fibrillar precursors crystallize and transform into shishes where the growth of kebabs is still suppressed because of the high temperature. With exact lattice matching and a good state of dispersion, shishes generated at these high temperatures are the ideal seeds for self-nucleation of the bulk material. For the deformation histories explored in this work, during cooling at 5 °C/min, shishes shift the onset of lamellar stacks, 124 °C in quiescent conditions, up to temperatures as high as 132 °C. Similar to efficient nucleating agents, the increase of the crystallization temperature is accompanied by the intrinsic ability to template oriented morphologies.

Our work demonstrates that, during cooling, the crystallization temperature of a polymer is a processing parameter that depends on the whole thermomechanical history, including deformations of the melt that take place in the vicinity of the equilibrium melting point.

ACKNOWLEDGMENT

The authors acknowledge ESRF and the Nederlandse Organisatie voor Wetenschappelijk Onderzoek (NWO) for granting the beamtime, the personnel of ID02 and BM26 of the ESRF for providing valuable help during the X-ray experiments and Dr.

Nilesh Kukalyekar for the synthesis of the materials. This work is part of the research program of the Dutch Polymer Institute (DPI), PO Box 902, 5600 AX Eindhoven, The Netherlands, project #634.

REFERENCES

(1) Wunderlich, B. *Macromolecular Physics*; Academic Press; New York, 1980.
(2) Muthukumar, M. *Adv. Chem. Phys.* **2004**, 128.
(3) Kristiansen, M.; Werner, M.; Tervoort, T.; Smith, P.; Blomehofer, M.; Schmidt, H. W. *Macromolecules* **2003**, *36*, 5150–5156.
(4) Marco, C.; Ellis, G.; Gomez, M. A.; Arribas, J. M. *J. Appl. Polym. Sci.* **2002**, *84*, 2440–2450.
(5) Menyhárd, A.; Gahleitner, M.; Varga, J.; Bernreitner, K.; Jääskeläinen, P.; Øysæde, H.; Pukánszky, B. *Eur. Polym. J.* **2009**, *45* (11), 3138–3148.
(6) Wittmann, J. C.; Lotz, B. *Polymer* **1989**, *30*, 27–34.
(7) Tsuji, H.; Tashiro, K.; Bouapao, L.; Narita, J. *Macromol. Mater. Eng.* **2008**, *293* (12), 947–951.
(8) Beck, H. N. *J. Appl. Polym. Sci.* **1967**, *11* (5), 673–685.
(9) Blomehofer, M.; Ganzleben, S.; Hanft, D.; Schmidt, H. W.; Kristiansen, M.; Smith, P.; Stoll, K.; Mader, D.; Hoffmann, K. *Macromolecules* **2005**, *38*, 3688–3695.
(10) Binsbergen, F. L. *Polymer* **1970**, *11* (5), 253–267.
(11) Kobayashi, T.; Hashimoto, T. *Bull. Chem. Soc. Jpn.* **2005**, *78*, 218–235.
(12) Li, H.; Huneault, M. A. *Polymer* **2007**, *48* (23), 6855–6866.
(13) Wittmann, J. C.; Lotz, B. *Polymer* **1981**, *19* (12), 1837–1851.
(14) Banks, W.; Gordon, M.; Sharples, A. *Polymer* **1963**, *4*, 289–302.
(15) Blundell, D. J.; Keller, A.; Kovacs, A. J. *J. Polym. Sci., Polym. Lett.* **1966**, *4*, 481–486.
(16) Fillon, B.; Wittmann, J. C.; Lotz, B.; Thierry, A. *J. Polym. Sci., Part B: Polym. Phys.* **1993**, *31* (10), 1383–1393.
(17) Mykhaylyk, O.; Chambon, P.; Graham, R. S.; Patrick, J.; Fairclough, A.; Olmsted, P. D.; Ryan, A. J. *Macromolecules* **2008**, *41* (6), 1901–1904.
(18) Seki, M.; Thurman, D. W.; Oberhauser, J. P.; Kornfield, J. A. *Macromolecules* **2002**, *35*, 2583–2594.
(19) Balzano, L.; Rastogi, S.; Peters, G. W. M. *Macromolecules* **2009**, *42* (6), 2088–2092.
(20) Azzurri, F.; Alfonso, G. C. *Macromolecules* **2008**, *41* (4), 1377–1383.
(21) Okada, K.; Washiyama, J.; Watanabe, K.; Sasaki, S.; Masunaga, H.; Hikosaka, M. *Polym. J.* **2010**, *42*, 464–473.
(22) Keller, A.; Kolnaar, H. W. H. Flow induced orientation and structure formation. In *Processing of Polymers*; Meijer, H. E. H., Ed.; VCH: New York, 1997; Vol. 18.
(23) Kumaraswamy, G.; Issaian, A. M.; Kornfield, J. A. *Macromolecules* **1999**, *32*, 7537–7547.
(24) Somani, R. H.; Yang, L.; Hsiao, B. S. *Physica A* **2002**, *304*, 145–157.
(25) Keum, J. K.; Zuo, F.; Hsiao, B. S. *J. Appl. Crystallogr.* **2007**, *40*, 48–51.
(26) Chai, C. K.; Dixon, N. M.; Gerrard, D. L.; Reed, W. *Polymer* **1995**, *36* (3), 661–663.
(27) Garcia Gutierrez, M.; Alfonso, G. C.; Riekel, C.; Azzurri, F. *Macromolecules* **2004**, *37*, 478–485.
(28) Sakellarides, S. L.; McHugh, A. J. *Rheol. Acta* **1987**, *26*, 64–77.
(29) Kanaya, T.; Takayama, Y.; Ogino, Y.; Matsuba, G.; Nishida, K. *Lect. Notes Phys.* **2007**, *714*, 87–96.
(30) Balzano, L.; Kukalyekar, N.; Rastogi, S.; Peters, G. W. M.; Chadwick, J. C. *Phys. Rev. Lett.* **2008**, *100*, 048302.
(31) Schultz, J. M. *Diffraction for Material Scientists*; Prentice-Hall: New York, 1982.
(32) Turner Jones, A.; Aizlewood, J. M.; Beckett, D. R. *Makromol. Chem.* **1964**, *75* (1), 134–158.
(33) Doi, M.; Edwards, S. F. *The Theory of Polymer Dynamics*; Clarendon Press: Oxford, 1986.
(34) Dealy, J. M.; Larson, R. G. *Structure and Rheology of Molten Polymers*; Hanser Gardner Publications: Cincinnati, 2006.
(35) Avrami, M. J. *Chem. Phys.* **1939**, *7* (12), 1103.
(36) Avrami, M. J. *Chem. Phys.* **1940**, *8*, 212–224.
(37) Avrami, M. J. *Chem. Phys.* **1941**, *9*, 177–184.
(38) Banks, W.; Sharples, A.; Hay, J. N. *J. Polym. Sci., Part A: Gen. Pap.* **1964**, *2* (9), 4059–4067.
(39) Kukalyekar, N.; Rastogi, S.; Chadwick, J. C. *Polym. Prepr.* **2007**, *48* (1), 280.
(40) Kukalyekar, N.; Balzano, L.; Peters, G. W. M.; Rastogi, S.; Chadwick, J. C. *Macromol. React. Eng.* **2009**, *3* (8), 448–454.
(41) Schultz, J. M. Polymer Crystallization. *The Development of Crystalline Order in Thermoplastic Polymers*, 1st ed.; Oxford University Press: Oxford, UK, 2001.
(42) Janeschitz-Kriegl, H. *Crystallization Modalities in Polymer Melt Processing: Fundamental Aspects of Structure Formation*; Springer: New York, 2009.
(43) Cho, T. Y.; Stille, W.; Strobl, G. *Macromolecules* **2007**, *40* (7), 2596–2599.
(44) Dukovski, I.; Muthukumar, M. *J. Chem. Phys.* **2003**, *118* (14), 6648–6655.
(45) Balzano, L.; Cavallo, D.; van Erp, T. B.; Ma, Z.; Housmans, J. W.; Fernandez-Ballester, L.; Peters, G. W. M. *IOP Conf. Ser: Mater. Sci. Eng.* **2010**, *14*, 012005.
(46) Cavallo, D.; Azzurri, F.; Balzano, L.; Funari, S.; Alfonso, G. C. *Macromolecules* **2010**, *43* (22), 9394–9400.
(47) Janeschitz-Kriegl, H.; Eder, G. *J. Macromol. Sci., Part B* **2007**, *46*, 591–601.
(48) Kimata, S.; Sakurai, T.; Nozue, Y.; Kasahara, T.; Yamaguchi, N.; Karino, T.; Shibayama, M.; Kornfield, J. A. *Science* **2007**, *316* (5827), 1014–1017.
(49) Baert, J.; Langouche, F.; Van Puyvelde, P. *Macromolecules* **2006**, *39*, 9215–9222.
(50) Kumaraswamy, G.; Verma, R. K.; Issian, A. M.; Wang, P.; Kornfield, J. A.; Yeh, F.; Hsiao, B. S.; Olley, R. H. *Polymer* **2000**, *41*, 8931–8940.
(51) Mykhaylyk, O. O.; Chambon, P.; Graham, R. S.; Fairclough, P. J.; Olmsted, P. D.; Ryan, A. J. *Macromolecules* **2008**, *41* (6), 1901–1904.
(52) Jerschow, P.; Janeschitz-Kriegl, H. *Rheol. Acta* **1996**, *35*, 127.
(53) Keum, J. K.; Burger, C.; Zuo, F.; Hsiao, B. S. *Polymer* **2007**, *48*, 4511–4519.
(54) Ruland, W. *J. Polym. Sci., Part C* **1969**, *28*, 143–151.
(55) Somani, R. H.; Yang, L.; Zhu, L.; Hsiao, B. S. *Polymer* **2005**, *46* (20), 8587–8623.
(56) Stribeck, N. *X-ray Scattering of Soft Matter*; Springer-Verlag: Berlin, 2007.
(57) Schultz, J. M.; Hsiao, B. S.; Samon, J. M. *Polymer* **2000**, *41* (25), 8887–889.
(58) Balzano, L.; Portale, G.; Peters, G. W. M.; Rastogi, S. *Macromolecules* **2008**, *41* (14), 5350–5355.
(59) Balzano, L.; Rastogi, S.; Peters, G. W. M. *Macromolecules* **2008**, *41*, 399–408.
(60) Nogales, A.; Mitchell, G. R.; Vaughan, A. S. *Macromolecules* **2003**, *36*, 4898–4906.
(61) Kavesh, S.; Schultz, J. M. *J. Polym. Sci., Part A-2: Polym. Phys.* **1971**, *9* (1), 85–114.
(62) Organ, S. J.; Keller, A. *J. Mater. Sci.* **1965**, *20* (5), 1602–1615.